MATERIALS RESEARCH SOCIETY
SYMPOSIUM PROCEEDINGS VOLUME 464

Dynamics in Small Confining Systems III

Symposium held December 2–5, 1996, Boston, Massachusetts, U.S.A.

EDITORS:

J.M. Drake
Exxon Research and Engineering Company
Annandale, New Jersey, U.S.A.

J. Klafter
Tel Aviv University
Tel Aviv, Israel

R. Kopelman
University of Michigan
Ann Arbor, Michigan, U.S.A.

MATERIALS RESEARCH SOCIETY
PITTSBURGH, PENNSYLVANIA

This work was supported in part by the Office of Naval Research under Grant Number ONR: N00014-97-1-0193. The United States Government has a royalty-free license throughout the world in all copyrightable material contained herein.

Single article reprints from this publication are available through University Microfilms Inc., 300 North Zeeb Road, Ann Arbor, Michigan 48106

CODEN: MRSPDH

Published by:

Materials Research Society
9800 McKnight Road
Pittsburgh, Pennsylvania 15237
Telephone (412) 367-3003
Fax (412) 367-4373
Website: http://www.mrs.org/

Library of Congress Cataloging in Publication Data

Dynamics in small confining systems III : symposium held December 2–5, 1996, Boston, Massachusetts, U.S.A. / editors, J.M. Drake, J. Klafter, R. Kopelman
p. cm—(Materials Research Society symposium proceedings ; v. 464)
Includes bibliographical references and index.
ISBN 1-55899-368-1
1. Molecular dynamics—Congresses. 2. Molecular structure—Congresses. 3. Surface chemistry—Congresses. I. Drake, J.M. II. Klafter, J. III. Kopelman, R. IV. Series: Materials Research Society symposium proceedings ; v. 464.
QD461.D947 1997 97-11467
530.4'17—dc21 CIP

Manufactured in the United States of America

DIFFUSION LIMITED WETTING

U. STEINER*,**, J. KLEIN*

*Department of Materials and Interfaces, Weizmann Institute of Science, Rehovot 76100, Israel
**Fakultät für Physik, Universität Konstanz, Postfach 5560, 78464 Konstanz, Germany

ABSTRACT

We have measured the growth with time t of a wetting layer (of thickness $l(t)$) at the surface of a thin film of a binary liquid (polymer) mixture. Over a wide range of experimental parameters, our data is well described by a model of diffusion limited wetting which takes into account the finite film thickness. In this model, $l(t)$ is a function of time which sensitively depends on the nature of the interfacial potential: a detailed comparison shows that long range van-der-Waals forces provide the main driving force for the build-up of the wetting layer .

INTRODUCTION

In many practical applications, the coating of a surface with a liquid film plays an important role. Paints, lubricants, adhesives and thin dielectric layers on semiconductors are a few examples where a surface is modified by a homogeneous macromolecular film. Together with a growing technological interest, there is an increasing activity in experimental and theoretical studies which try to elucidate the thermodynamic origin of wetting phenomena and thin film stability [1-15]. For the surface modification of a of a polymeric surface by a macromolecular layer, for example, thin film stability may be a problem [16,17] Following Cahn's argument [18], this may be related to the intrinsic immiscibility of binary polymer liquids (α, β): starting from Young's equation [19], which relates the contact angle θ of a liquid α with a surface to the three surface tensions $\gamma_{\alpha s}$, $\gamma_{\beta s}$ and $\gamma_{\alpha\beta}$:

$$\cos(\theta) = \frac{\gamma_{as} - \gamma_{\beta s}}{\gamma_{\alpha\beta}} \qquad (1)$$

the balance between the three surface tensions determines whether a liquid α forms a continuous film on a surface s ($\gamma_{\alpha\beta} >= \gamma_{\alpha s} - \gamma_{\beta s}$) or whether such a film is unstable ($\gamma_{\alpha\beta} < \gamma_{\alpha s} - \gamma_{\beta s}$). As the critical temperature T_c for phase separation is approached, both terms ($\gamma_{\alpha\beta}$, $\gamma_{\alpha s} - \gamma_{\beta s}$) approach zero. But whereas the interfacial energy of the liquid–liquid interface vanishes with the critical exponent of the bulk correlation length $\gamma_{\alpha\beta} \sim (T_c - T)^{1.3}$, the difference of the liquid-surface interfacial energies scale with a critical surface exponent $(\gamma_{\alpha s} - \gamma_{\beta s}) \sim (T - T_c)^{0.8}$. Since the numerator of Eq. (1) approaches zero more rapidly than the denominator, a transition from partial wetting (drops of the α-phase on the surface) to complete wetting (a thick continuous film of the α-phase on the surface) is expected to occur. Inversely, immiscible liquids far from their critical point T_c are likely to be in the partial wetting regime, and continuous films delimiting a macromolecular bulk from a surface are unstable and tend to break-up [16].

The Cahn argument, however, is valid in this simplified version only if short-range interactions are the dominant driving forces at the surface. Competing long- and short range interfacial forces may suppress complete wetting near the critical point, or lead to a wetting layer even far from T_c [2]. The question whether long-range forces contribute to the wetting layer formation may therefore be of considerable importance when investigating thin film stability of polymer layers. The integrated amount of one of the coexisting phases near a surface (surface excess) yields some information on the thermodynamics of the surface layer [6,20]. The predictions based on these measurements concerning the wetting transition, however, are dependent on the theoretical model used in the data analysis. In particular, there is no

Mat. Res. Soc. Symp. Proc. Vol. 464 © 1997 Materials Research Society

unambiguous way to extract in a model independent way the type of surface interaction (long-range or short-range) from an equilibrium absorption experiment.

A novel approach which provides information on the nature of the surface potential is the measurement of the build-up of a surface layer with time [21]. Theoretical studies of diffusion limited wetting layer growth predict different functional forms for the growth of the surface layer thickness with time, depending on the surface potential that drives the process [11,12]. While measurements of dynamic properties in liquids are difficult to perform, since the presence of convectional effects and gravitational fields complicate the surface layer kinetics, these effects are negligible for small polymer melt samples. This allows the application of models which assume strictly diffusion-limited growth in order to extract surface potentials.

Here we report the experimental observation of a wetting layer build-up from a binary polymer mixture with time. We develop a theoretical model to describe the diffusion limited growth of a wetting layer in a confined geometry. In the last section, we describe the analysis of the experimental data in the framework of this theory.

EXPERIMENT

Materials and Sample Preparation

The polymers used in this work are statistical copolymers made of ethylene and ethyl-ethylene monomers (PE-PEE): $([C_4H_8]_{1-x} - [C_2H_3{-}(C_2H_5)]_x)_N$. Binary mixtures of such polymers (A, B) with values of $\Delta x = x_A - x_B$ from 0.9 to 0.14 and molecular weights N from 1510 – 2030 have been shown to be partially miscible with critical temperatures in the range from 33 – 223°C [22]. For such couples the higher-x containing polymer shows a pronounced enrichment at the free (air) interface, and complete wetting of the sample surface by this component has been found for several binary pairs [6,22]. To allow detection by the experimental technique described in next paragraph, the higher-x component was partially deuterated. The details of the polymers used are summarized in Table I. Two polymer couples were used in this study: *d*88/*h*78 and *d*66/*h*52. The bulk properties of these couples have been studied before. Their critical temperatures are: T_c = 127°C (*d*88/*h*78) and T_c = 204°C (*d*66/*h*52) [22].

Samples were prepared by spin-coating a film from toluene solution onto a polished silicon surface, which in some cases was covered by a thin gold layer to improve thin-film stability. A second film was similarly spin-cast onto freshly cleaved mica. To obtain bilayers, the film was floated from mica onto the first film. Since the PE-PEE polymers are liquid at room temperature (their glass transition temperature is < –40 °C), a jig was developed for depositing the film from the mica onto the substrate (Fig. 1). As the jig is lowered below the water surface, water intercalates between the polymer film and the mica and the film is pushed onto the substrate. Thus, at each instant, only a very short segment of the film is suspended from the mica surface. This avoids the shrinking and thickening which occurs when a hyrophobic liquid film is floated entirely onto a water surface prior to being transferred to the other surface.

Sample series were annealed in a vacuum oven (< 10^{-2} Torr) at temperatures T between 45 – 163 °C (± 0.3 °C), for times t from 15 min. to 1 month. After annealing, the samples were quenched in liquid nitrogen and stored at -80°C. Each sample was annealed once only for a given time t, and its concentration profile was analyzed by nuclear reaction analysis.

TABLE I. Characteristics of the $([C_4H_8]_{1-x} - [C_2H_3{-}(C_2H_5)]_x)_N$ .statistical copolymers. x is the ethyl-ethylene content, N the degree of polymerization and f_D the fractional deuteration.

Sample	x	N	f_D
*d*88	0.88	1610	0.34
*h*78	0.78	1290	0.00
*d*66	0.66	2030	0.40
*h*52	0.52	1510	0.00

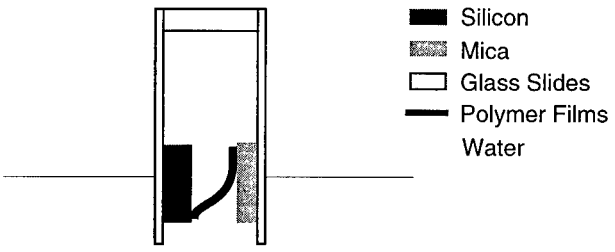

Fig. 1. Jig to create bilayers from polymers which are liquid at room temperature. As the jig is lowered into the water, the polymer film floats off the mica and is immediately brought into contact with the film on the silicon substrate. The separation between the silicon and mica substrates is typically less than 1 mm.

Nuclear Reaction Analysis

To obtain the concentration-depth profiles $\phi(z)$ of the deuterated polymer species, nuclear reaction analysis (NRA) was employed [23]. NRA is based on the $^3He + ^2H \rightarrow ^4He + ^1H +$ 18.35 MeV nuclear reaction. The experimental set-up is schematically represented in Fig. 2. A 900 keV ^3He beam is incident on the polymer sample. As the ^3He ions penetrate the polymer film, they lose energy due to inelastic electronic interactions. This results in a lowered energy of the ^4He particles as compared to a nuclear reaction which takes place at the sample surface. The outgoing α-particles additionally lose energy traversing the film *en route* to the detector, and the overall energy loss is directly related to the depth z at which the reaction has taken place. By measuring the energy spectrum of the high energy $^4He^{++}$ ions, a concentration-depth profile $\phi(z)$ can directly be computed, after correcting for the reaction cross-section of the $^2He(^3He,^4He)^1H$ nuclear reaction.

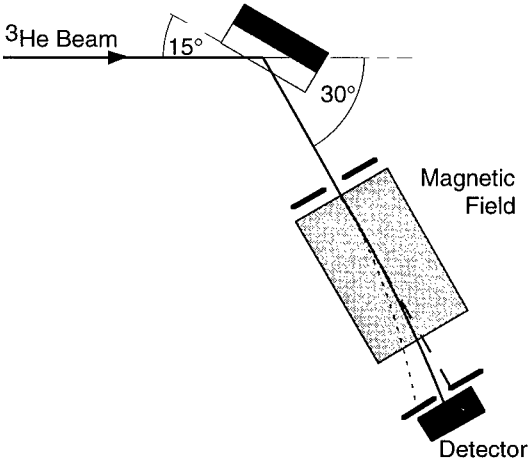

Fig. 2. Schematic representation of the nuclear reaction analysis experiment. A ^3He beam is incident onto the sample where the $^3He+^2H\rightarrow^4He+^1H$ nuclear reaction takes place. A magnetic filter admits only the $^4He^{++}$ ions to the detector. The $^4He^{++}$ energy spectrum can directly be converted into a depth-concentration profile of the deuterated polymer in the sample.

RESULTS

Concentration-depth profiles of an annealing series are shown in Fig. 3 for *d*66/*h*52 bilayers at an annealing temperature of $T = 110$ °C. In the unannealed sample the polymer layer which is higher in PEE content is initially on the silicon substrate, and is thus excluded from the air-surface, where the wetting layer is expected to form, by the PEE-poorer layer (Fig. 3a). Upon annealing for $t = 18$ h (Fig 3b), the two layers have partially interdiffused and the two coexisting concentrations $\phi_1 \approx 0.75$ and $\phi_2 \approx 0.25$ are established, separated by an interface whose width is given by the correlation length ξ ($\approx$ 22 nm). At the same time, a narrow surface peak of the phase rich in *d*66 (the surface-preferred component) appears at the air interface. For increasing annealing times ($t = 190$ h (Fig. 3c) and $t = 720$ h (Fig 3d)), the width l of the surface peak increases, forming a wetting layer of composition $\phi_s \approx \phi_1$. The formation of a surface layer of width $l >> \xi$ is direct evidence for complete wetting, and the growth of the wetting layer is only limited by the overall material available to be incorporated into the surface layer. In this experiment, the *d*66 layer next to the substrate surface acts as a reservoir, which supplies the *d*66 chains which are incorporated into the wetting layer. A sample consisting of a uniform film of composition ϕ_1 would quickly be depleted to a concentration $\phi < \phi_1$ for $z >> l$ and the increase of l would come to a stop. It should be mentioned that gravitational effects are negligible for these thin films, and convectional flow is suppressed by the high viscosity of the polymer melts.

In Fig. 4, the raw data of the wetting layer thickness l versus annealing time t is displayed on double logarithmic scales for the *d*88/*h*78 couple [Fig 4(a)] and the *d*66/*h*52 couple [Fig. 4(b)]. In Fig. 4(a), the diffusion temperature was kept constant at $T = 110$ °C, but the thicknesses of the *h*78 layer of the unannealed sample was varied. In Fig. 4(b), the sample layer thicknesses, as well as the annealing temperatures was varied in the different data sets. While a direct interpretation of these raw data seems difficult in the case of Fig. 4(b), a model which takes the

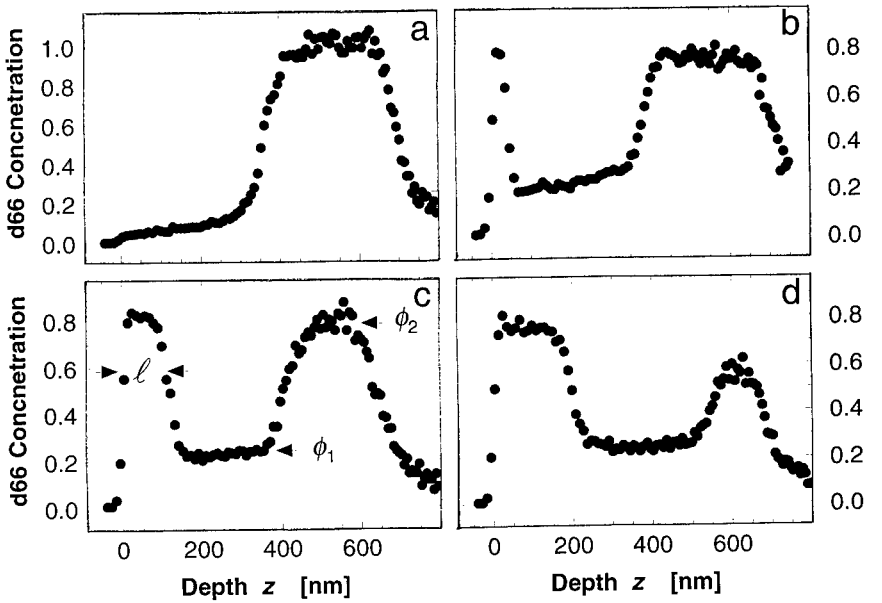

FIG. 3. Concentration-depth profiles for the *d*66/*h*52 couple annealed at 110°C, determined by nuclear reaction analysis; (a) unannealed, (b) after 18h, (c) after 190h and (c) after 720h. The glass transition temperature for this couple is ca. -60 °C, and some interdiffusion can be observed in the unannealed sample due to the sample handling at room temperature.

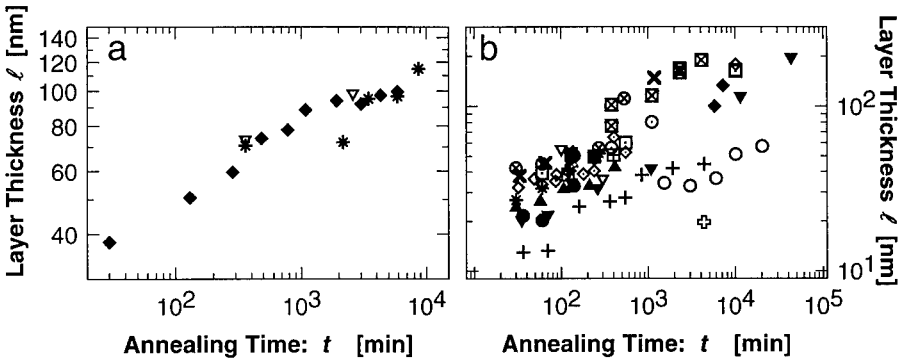

FIG. 4. Wetting layer thickness l vs annealing time t; (a) $d88/h78$ annealed at 110°C. The different symbols refer to varying sample geometries d: ✱, d = 315 – 530 nm; ▽, d = 360 nm; ◆, d = 270– 340 nm. (b) $d66/h52$. The different symbols refer to varying sample geometries d and varying temperatures: ✖, T = 163 °C, d = 345 nm; ✚, T = 160 °C, d = 340 nm; ⊗, T = 154 °C, d = 215 nm; ⊕, T = 151 °C, d = 130 nm; ⊞, T = 150 °C, d = 590 – 670 nm; ◇, T = 150 °C, d = 500 – 680 nm; ⊙, T = 150 °C, d = 500 – 650 nm; ⊡, T = 150 °C, d = 545 nm; ▽, T = 150 °C, d = 510 nm; ◇, T = 150 °C, d = 310 nm; △, T = 150 °C, d = 250 nm; □, T = 149 °C, d = 325 nm; ✱, T = 140 °C, d = 120 – 250 nm; ▼, T = 110 °C, d = 335 nm; ◆, T = 110 °C, d = 315 nm; ▲, T = 110 °C, d = 175 nm; ●, T = 110 °C, d = 130 nm; +, T = 90 °C, d = 330 nm; ○, T = 70 °C, d = 275 nm; ✣, T = 45 °C, d = 260 nm.

diffusion limited growth of the wetting layer into account is developed in the following section.

DIFFUSION LIMITED WETTING LAYER GROWTH

Excluding the initial stages, where bulk-equilibrium is established, and the initial interfacial build-up occurs, we consider three different regions in the composition profile, as indicated schematically in Fig. (5): (I) The wetting layer of plateau concentration $\phi_s \approx \phi_2$ and thickness l; (II) the non-wetting phase adjacent to (I) of width d and compositions ranging from ϕ_d to ϕ_1; (III) the "reservoir" phase of composition ϕ_2. In our model, we take the material transport to be diffusion limited, but make the reasonable assumption that the wetting layer (I) is in local equilibrium with the immediately adjacent region of concentration ϕ_d. That is, the transfer of material from to the wetting layer from the immediately adjacent region is rapid compared with the flux of material from the reservoir to the wetting layer. When the wetting layer is formed, the adjacent region is depleted, resulting in a concentration gradient in region II, and the growth of the wetting layer is fed by the flux through region II. Since the form of the interfacial composition gradient between region II and III is fixed by the bulk-thermodynamic parameters, mass-transport through region II can occur only by translating the II–III interface towards greater values of z. For a wetting layer thickness l larger than the bulk-correlation length ξ, the composition of the wetting layer ϕ_s becomes approximately equal to ϕ_2. Since $\phi_d \approx \phi_1$, conservation of mass requires that the width of region II, d, be conserved, as indeed seen from the composition profiles in fig. 3. Mass–transport with time is then given by the flux-equation, which relates the increase with time of the surface excess to the flux through region II:

$$\frac{d}{dt}\left[(\phi_2 - \phi_1)\,(l(t) - l(0))\right] = \frac{D(\phi_1, T)}{d}(\phi_1 - \phi_d) \qquad (2)$$

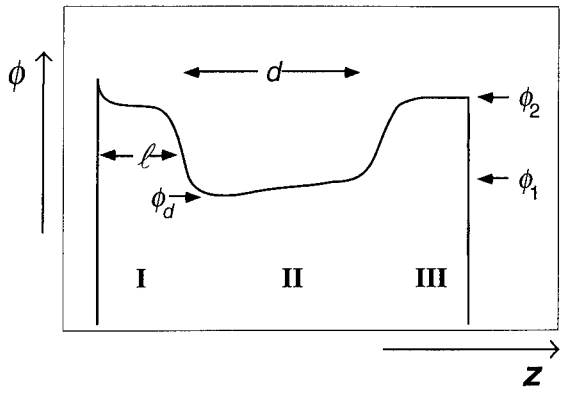

FIG. 5. Schematic representation of the model presented in the text. The composition profile is divided into three regions: (I) the wetting layer of thickness *l* in local equilibrium with the adjacent phase of composition ϕ_d; (II) the diffusion gradient $\phi_1 - \phi_d$; and (III) the reservoir phase of composition ϕ_2. The increase of the wetting layer takes place by diffusion of polymers from the reservoir phase (III) via the concentration gradient (II) into the wetting layer (I).

where $D(\phi, T)$ is the mutual diffusion coefficient. Since $\phi_d \approx \phi_1$, diffusion takes place in the close vicinity of the phase boundary, and thermodynamic slowing down of diffusion has to be taken into account, leading to a composition dependent diffusion coefficient. To eliminate ϕ_d from Eq. (2), $(\phi_1 - \phi_d)$ can be expressed in terms of the relative chemical potential [11]:

$$\left(\phi_1 - \phi_d\right) = \left[\mu(\phi_1, T) - \mu(\phi_d, T)\right]\left(\frac{\partial \mu}{\partial \phi}\right)^{-1}_{\phi=\phi_1} \tag{3}$$

The chemical potential difference can be related to the interfacial potential $V(l)$ per unit area [11]:

$$\rho(\phi_2 - \phi_1)\left[\mu(\phi_1, T) - \mu(\phi_d, T)\right] = -\frac{\partial V}{\partial l} \tag{4}$$

where $\rho = (1/a^3)$ the monomer number density with a is the statistical segment size. Eqs. (2) - (4) can be combined to yield a differential equation which describes the growth with time of the wetting layer as a function of the derivative of the surface potential:

$$\frac{dl}{dt} = -\left(\left.\frac{\partial \mu}{\partial \phi}\right|_{\phi_1} (\phi_2 - \phi_1)^2\right)^{-1} D(\phi, T)\,\frac{1}{\rho d}\,\frac{\partial V(l)}{\partial l} \tag{5}$$

Equation 5 can be simplified by writing out expressions for $D(\phi)$ and $\partial\mu / \partial\phi$. An expression for the diffusion coefficient which takes the thermodynamic slowing-down into account is given by [24,25]:

$$D(\phi) = \Omega(\phi)\left[\chi_s(\phi) - \chi\right] \tag{6}$$

$\Omega(\phi)$ is a mobility term:

$$\Omega(\phi) = 2\phi(1-\phi)\left[D_a^* N_a (1-\phi) + D_b^* N_b \phi\right] \tag{7}$$

and $\chi_s(\phi)$ is the value of the Flory-Huggins interaction parameter χ on the spinodal:

$$\chi_s(\phi) = \frac{1}{2}\left(\frac{1}{N_a\phi} + \frac{1}{N_b(1-\phi)}\right) \tag{8}$$

N_a and N_b are the polymerization indices of the two polymers, and D_a^* and D_b^* their respective tracer diffusion coefficients.

The chemical potential can be evaluated from the standard Flory-Huggins energy functional for polymer mixing to yield the chemical potential derivative [26]:

$$\frac{\partial\mu}{\partial\phi} = \left[\frac{1}{N_a\phi} + \frac{1}{N_b(1-\phi)} - 2\chi\right]k_BT \tag{9}$$

where k_B is Boltzmann's constant. Equations (6) – (9) define an effective mobility Ω_{eff}:

$$\Omega_{eff}(\phi_1,\phi_2,T) = \left(\left.\frac{\partial\mu}{\partial\phi}\right|_{\phi_1}(\phi_2-\phi_1)^2\right)^{-1} D(\phi,T) = \frac{\phi_1(1-\phi_1)\left[D_a^*N_a(1-\phi_1) + D_b^*N_b\phi_1\right]}{k_BT(\phi_2-\phi_1)^2} \tag{10}$$

Equation (5) then becomes:

$$\frac{dl}{dt} = -\frac{\Omega_{eff}}{\rho d}\frac{\partial V(l)}{\partial l} \tag{11}$$

Note that by combining Eqs. (6) and (9), all explicit references to the interaction parameter χ cancel, reducing Eq. (11) to a diffusion problem which depends only on the surface potential $V(l)$ and the diffusion geometry as indicated in Fig. 5.

To analyze our experimental data in the framework of the present model, we consider three different forms for $V(l)$:

$$V(l) = -\frac{A_s}{a^2}\exp\left(-\frac{l}{\zeta}\right) \qquad \text{(short range)} \tag{12a}$$

$$V(l) = -\frac{A_{nr}}{12\pi l^2} \qquad \text{(non-retarded vdW)} \tag{12b}$$

$$V(l) = -\frac{aA_r}{l^3} \qquad \text{(retarded vdW)} \tag{12c}$$

where the coefficients A_s, A_{nr} and A_r have units of energies and are the effective surface interaction potentials. Equation (12a) describes a short-range surface interaction which decays exponentially with a decay length which is expected to be short-ranged, i.e. $\zeta \approx a$. A_s is often given by an expansion [27]: $A_s = 1/\zeta\ (\mu_1\ \phi_s + 0.5\ g\ \phi_s^2)\ k_BT$, with μ_1 a chemical potential difference, favoring the component which forms the wetting layer, and g a prefactor to the quadratic term in ϕ_s, which takes changes of interactions due to the presence of the surface ("missing neighbors") into account. Equation (12b) represents non-retarded van der Waals interactions (vdW) with A_{nr} the non-retarded Hamaker constant. For large values of l, retardation effects are expected to play a role and a potential for retarded vdW interactions [Eq. (12c)] must be used, with an effective retarded Hamaker constant A_r. Substitution of Eqs. (12) into Eq. (11) yields the time dependence of the wetting layer growth:

$$\frac{l(t)}{a} = \log\left(\frac{-A_s a \Omega_{eff} t}{d\zeta^2}\right) \qquad \text{(short range)} \qquad (13a)$$

$$\frac{l(t)}{a} = \left(\frac{-2A_{nr}}{3\pi}\frac{\Omega_{eff} t}{da}\right)^{\frac{1}{4}} \qquad \text{(non-retarded vdW)} \qquad (13b)$$

$$\frac{l(t)}{a} = \left(\frac{-A_r}{15}\frac{\Omega_{eff} t}{da}\right)^{\frac{1}{5}} \qquad \text{(retarded vdW)} \qquad (13c)$$

Note that Eqs. (13) predict a qualitative difference for the case of short-range interactions (logarithmic growth-law) and long-range vdW interactions (power-law). The derivation of the present theoretical model follows the treatment by Lipowski and Huse (LH), for wetting from a semi-infinite phase of composition ϕ_1 (i.e. $d \rightarrow \infty$ in Fig. 5) [11,12]. While their predictions for the short-range case also features a logarithmic time dependence of the wetting layer, their exponents in the case of vdW interactions differ from the results in Eqs. (13): LH find exponents of $^1/_8$ and $^1/_{10}$ for non-retarded and retarded vdW interactions respectively, to be contrasted with our values of $^1/_4$ and $^1/_5$. This is a consequence of the different model geometries. In the LH model the depletion zone which establishes the diffusion gradient extends spatially with time to depths $z \approx \sqrt{(Dt)}$, and is quite inappropriate for the present thin film geometry [28]. In contrast, the diffusion distance in the present model between reservoir and wetting layer is fixed, leading to an accelerated material transport.

DISCUSSION

The form of Eqs. (13) suggests the use of transformed the length and time coordinates: $l \rightarrow l/a$ and $t \rightarrow \Omega_{eff} t/ad$. The use of these rescaled coordinates allows us to superimpose data sets measured at different temperatures and samples of different sample geometry (i.e. d values). In Fig 6 we plot the data from Fig. 4 using rescaled coordinates. In Fig. 6(a) and (c), the wetting layer thickness l is plotted versus a reduced time t/d for the $d88/h78$ data sets. Here, annealing was carried out at a fixed temperature of 110 °C, leading to a constant value of the effective mobility Ω_{eff}, and only the value of d was varied in a range from 270 to 530 nm.

In the case of the $d66/h52$ couple [fig. 6(b) and (d)], the temperature as well as diffusion distance d was varied and the coordinate transformation as mentioned above (l/a vs. $\Omega_{eff} t/ad$) was used. For the data reduction, values for the statistical segment length a were taken from ref. [29], and the mobility Ω_{eff} was computed from Eq.(10). The required parameters in Eq. (10), ϕ_1 and ϕ_2 could in principle be obtained directly from the composition profiles, but more precise values from ref. [22] are used. The tracer diffusion coefficients D^* were estimated via their mutual diffusion coefficients D^{mut} (e.g. for tracer diffusion of $d66$ in $h52$: $D^*_{d66} \approx D^{mut}_{h52}$). The mutual diffusion coefficients for $d66$ and $h52$ have been measured by analyzing the diffusion profiles of $d66/h66$ and $d52/h52$ at room temperature [30]. To obtain the values of D^{mut} at the annealing temperatures of this study, a WLF extrapolation was performed, using the WLF parameters from ref. [30].

Comparing Fig. 4(a) and Fig 6(a) and(c) only a minor reduction of the scatter in the data is detected, when using reduced coordinates. In Fig. 6(d), however, the large scatter in fig. 4 collapses strikingly to give a single master curve which includes all data. To compare the experimental data to Eqs. (13), the data are plotted on log-linear [Fig. 6(a) and 6(b)] and on a double logarithmic scale [Fig. 6(c) and 6(d)]. For $d88/h78$, within the small range in reduced time (2 orders of magnitude), the data is equally well described by a linear relation for both representations. This is a general feature of weak power laws, which resemble logarithmic laws unless a sufficient dynamic range of variables is available. The $d66/h52$ data set exhibits a linear representation only on a double logarithmic scale (Fig. 6d), while the log-linear plot [Fig. 6(b)]

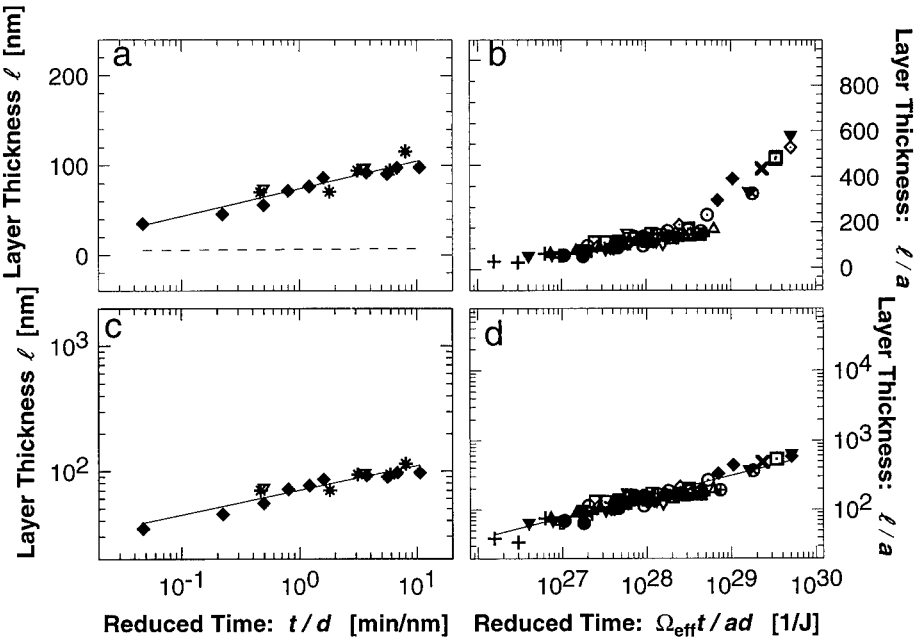

FIG. 6. Time dependence of wetting layer thickness from Fig. 4 in reduced coordinates (the symbols are the same as in Fig. 4): (a) and (c): l vs t / d for the $d88/h78$ couple; (b) and (d): l/a vs $\Omega_{eff}t / da$ for the $d66 / h52$ couple. Plot (a) and (b) are in a log – linear representation, (c), (d) on a double-logarithmic scale. The solid line in (a) is a fit to the relation $l \propto \log(t / d)$, the dashed line is the theoretically predicted variation of l with time (see text). The solid line in (c) and (d) are the power-law relations: (c) $l \propto (t / d)^{0.20}$ and (d) $l / a \propto (\Omega_{eff}t / da)^{0.30}$.

shows a distinct curvature, indicating that a long-range surface interaction [Eqs. (12b) and (12c)] rather than a short range potential better describes the experimental data.

To proceed, power-law fits were performed on the data of Fig. 6(c) and (d) (straight lines in the double-logarithmic representation). The solid line in Fig 6(c) corresponds to a power-law relation: $l \sim (t / d)^{\kappa}$, with $\kappa = 0.20 \pm 0.05$. In Fig. 6(d), the corresponding power-law fit: $l/a \sim (\Omega_{eff}t / ad)^{\kappa}$ yields $\kappa = 0.30 \pm 0.05$. While the power-law exponent κ of the fit in Fig. 6(c) is close to the prediction of Eqs. (13b) or (13c), the uncertainty in the exponent κ is too large to distinguish between the two cases. In any event, one does not expect a sharp crossover in behaviour when non-retarded go over to retarded interactions. The exponent κ for the $d66/h52$ data set [Fig. 6(d)] lies somewhat above the values predicted by Eqs. (13b) and (13c). This discrepancy may be due to the uncertainties in the values of the parameters used in the data reduction (a, ϕ_1, ϕ_2, and Ω_{eff}). In particular the temperature extrapolation of the tracer diffusion coefficients D^*, which enter in the calculation of Ω_{eff} is likely to introduce some error in Ω_{eff} for the higher temperatures. Fitting the data in Fig 6(c) and 6(d) with the non-retarded power-law from Eq. (13b) (the exponent $\kappa = 0.25$ lies within the error margin of both fits described above), using the Hamaker constant A_{nr} as adjustable parameter, we obtain values for $-A_{nr}$ in the range from 10^{-20} to 10^{-21} J, with the uncertainty resulting from the scatter in our data. These values of

A_{nr} compare well with Hamaker constants of non-polar liquids. Taken together with the power law fit to the data, this strongly implicates long-range forces as driving the growth of the wetting layer.

A similar analysis can be performed for Fig. 6(a), but in this case a very different picture emerges. We find that despite the apparent fit to a logarithmic variation $l \propto \log(t)$ (Fig. 6a), the *slope* of the data, using the decay length ζ as a fit parameter of the data to eq. (13a), yields a value $\zeta \approx 31$nm. Since eqs. (12a) and (13a) correspond to a short range interfacial potential, ζ must be comparable to a monomer size or the statistical segment length $a \approx 6$ Å. Thus eqs. (12a) and (13a) *cannot* provide a consistent quantitative description of the $l(t)$ data.

Previous experimental studies on the equilibrium properties of surface enriched layers of the *d*66/*h*52 couple also find deviations from the Cahn model of wetting which assumes a short range interfacial potential [7,20]. One of these studies provide an estimation for the short-range interaction strength for two PE-PEE systems [20]. Using their published data we obtain an estimate for A_s: $A_s \approx -0.05 k_B T$, and taking the decay-length $\zeta = a \approx 6$Å, a prediction for the growth of a wetting layer which is driven uniquely by short-range interactions [Eq. (12b)] can be calculated The result of this calculation is indicated by the dashed line in Fig. 6(a). The theoretically predicted growth of the wetting layer $l(t)$ lies significantly lower than the data points. After 6 days, the longest annealing time for the *d*88/*h*78 couple, the theoretically predicted value $l \approx 7$ nm is smaller than the bulk correlation length which sets a lower limit to the validity of our model. In order to attain a 100 nm layer in the framework of this model, using the experimental parameters listed above, cosmological times (10^{60}–10^{120} years) would be required. Thus, while it may well be that short range effects contribute to surface segregation and enrichment of the surface-preferred species, they can play only a negligible role in driving the growth of the wetting layer.

CONCLUSIONS

Using a ion-beam depth-profiling technique, we have investigated the growth with time of a wetting layer from binary polymer mixtures. In the absence of gravitational effects and convectional flow, we propose a model in which the growth of the wetting layer is limited by diffusion from a reservoir at a fixed distance. Since this model makes no *a priori* assumptions on the interaction potential, it is possible to distinguish unambiguously between different surface potentials which drive the formation of the wetting layer.

Applying this model to our experimental data, measurements taken with a variety of different experimental parameters collapse to a single master curve. The functional form of the master curve: $l(t) \sim t^K$ is a signature of a wetting layer formation driven by van der Waals forces; while discrimination between this form and a logarithmic variation (indicating short-ranged forces) is possible, the dominance of long-ranged fields is strongly corroborated by a quantitative analysis which yields a Hamaker constant in the order $10^{-20} - 10^{-21}$ J, a value which is common for non-polar liquids. We show that any short-ranged interactions (which act on the length scale of a monomer size) play only a minor role, and contribute negligibly to the build-up of the wetting layer.

Since most surface aggregation experiments from binary polymer mixtures exhibit similar parameters for the short-range surface free energy, the present model suggests that van der Waals interaction are essential to form macroscopic wetting layers.

Finally, we point out that the study of the dynamics of wetting layer formation provides an tool which allows assess the precise form of surface potentials in polymeric liquids. This technique could complement equilibrium absorption studies[20], where such a distinction between different surface potentials is more difficult to achieve.

ACKNOWLEDGEMENTS

We especially thank Lew Fetters for providing the polymers used in this work, and David Andelman, Kurt Binder, Reinhard Lipowski and Sam Safran for discussions. Partial support from the German Israel Foundation, the Minerva Foundation, the Commission of the European

Community, the Ministry of Science and Arts (Israel) and the Kernforschungszentrum (Julich) is gratefully acknowledged.

REFERENCES

1. R. F. Kayser, M. R. Moldover, and J. W. Schmidt, J. Chem. Soc. Faraday Trans. II **82**, 1701 (1986).

2. S. Dietrich, in *Phase Transitions and Critical Phenomena* , edited by C. Domb, and J. L. Leibiwitz (Academic Press Limited, New York, 1988), Vol. XII, p. 1-218.

3. X. L. Wu, M. Schlossman, and C. Franck, Phys. Rev. B **33**, 402 (1986).

4. P. Guenon, and D. Beysens, Phys. Rev. Lett. **65**, 2406-2409 (1990).

5. P. Wilzius, and A. Cumming, Phys. Rev. Lett. **66**, 3000 (1991).

6. U. Steiner, J. Klein, E. Eiser, A. Budkowski, and L. Fetters, Science **258**, 1126-1129 (1992).

7. F. Bruder, and R. Brenn, Phys. Rev. Lett. **69**, 624 (1992).

8. B. Q. Shi, C. Harrison, and A. Cumming, Phys. Rev. Lett. **70**, 206 (1993).

9. B. M. Law, Phys. Rev. Lett. **72**, 1698 (1994).

10. U. Steiner, J. Klein, and L. J. Fetters, Phys. Rev. Lett. **72**, 1498-1501 (1994).

11. R. Lipowsky, Phys. Rev. B **32**, 1731 (1985).

12. R. Lipowsky, and D. A. Huse, Phys. Rev. Lett. **57**, 353-356 (1986).

13. K. K. Mon, K. Binder, and D. P. Landau, Phys. Rev. B **35**, 3683 (1987).

14. R. A. L. Jones, L. J. Norton, E. J. Kramer, and F. S. Bates, Phys. Rev. Lett. **66**, 1991 (1991).

15. G. Krausch, C.-A. Dai, E. J. Kramer, and F. S. Bates, Phys. Rev. Lett. **71**, 3669 (1993).

16. F. Brochard-Wyart, and F. Daillant, J. Canad. J. Phys. **68**, 1084 (1990).

17. G. Reiter, Phys. Rev. Lett. **68**, 75 (1992).

18. M. Schick, in *Liquids at Interfaces* , edited by J. Charvolin, and J.-F. Joanny (North Holland, Amsterdam, 1990), Vol. p. 419-497.

19. T. Young, Phil. Trans. Roy. Soc. London **95**, 65 (1805).

20. F. Scheffold, A. Budkowski, U. Steiner, E. Eiser, J. Klein, and L. J. Fetters, J. Chem. Phys. **104**, 8795 (1996).

21. U. Steiner, and J. Klein, Phys. Rev. Lett. **77**, 2526 (1996).

22. F. Scheffold, E. Eiser, A. Budkowski, U. Steiner, J. Klein, and L. J. Fetters, J. Chem. Phys. **104**, 8786 (1996).

23. U. K. Chaturvedi, U. Steiner, O. Zak, G. Krausch, G. Schatz, and J. Klein, Appl. Phys. Lett. **56**, 1228-1230 (1990).

24. R. J. Composto, E. J. Kramer, and D. M. White, Nature **328**, 234 (1987).

25. A. Losch, D. Wörmann, and J. Klein, Macromolecules **27**, 5713-5715 (1994).

26. P. J. Flory, *Principles of Polymer Chemistry* (Cornell University Press, Ithaca, 1953).

27. I. Schmidt, and K. Binder, J. Phys. II(Paris) **46**, 1631 (1985).

28. U. Steiner, J. Klein, E. Eiser, A. Budkowski, and L. J. Fetters, Berichte der Bunsengessellschaft für Physikalische Chemie **98**, 366 (1994).

29. N. P. Balsara, L. J. Fetters, N. Hadjichristidis, D. J. Lohse, C. C. Han, W. W. Graessley, and R. Krishnamoorti, Macromolecules **25**, 6137 (1992).

30. A. Losch, R. Salomonovic, U. Steiner, L. J. Fetters, and J. Klein, J. Polym. Sci., Polym. Phys. **33**, 1821-1831 (1995).